CARBON ATMOSPHERIC TRACER RESEARCHTO IMPROVE NUMERICAL SCHEMES AND EVALUATION

CATRINE

Carbon Atmospheric Tracer Research to Improve Numerics and Evaluation

D3.2 Impact of boundary conditions

Due date of deliverable	30 April 2025
Submission date	20 May 2025
File Name	CATRINE-D3.2-V1.0
Work Package /Task	WP3 / Task 3.1
Organisation Responsible of Deliverable	URCA
Author name(s)	T. Lauvaux, A. Rafalimanana, A. Raznjevic, M. Krol
Revision number	1.0
Status	Issued
Dissemination Level / location	Public

Funded by the European Union

The CATRINE project (grant agreement No 101135000) is funded by the European Union.
Views and opinions expressed are however those of the author(s) only and do not necessarily reflect those of the European Union or the Commission. Neither the European Union nor the granting authority can be held responsible for them.

1 Executive Summary

The Carbon Atmospheric Tracer Research to Improve Numerical schemes and Evaluation (CATRINE) project aims to evaluate and improve the numerical schemes for tracer transport in the new Copernicus anthropogenic CO_2 emissions Monitoring and Verification Support capacity (CO2MVS) and more widely in the Copernicus Atmosphere Monitoring Service (CAMS). The CO2MVS capacity will combine information from satellite and in-situ observations with detailed computer simulations of the atmosphere and biosphere to estimate anthropogenic emissions and sinks of CO_2 and CH_4. This combination of observations and modelling in an integrated system approach provides the added value to what we already know in terms of emissions and sinks from human activities, by consistently monitoring CO_2 and CH_4 emissions in much more detail, both in space and time.

While high-resolution models make a better connection between point sources and atmospheric observations, and are therefore better suited to estimate emissions, several technical challenges remain regarding the assimilation of isolated plumes from cities and large industries. Higher-resolution models can better resolve the emission patterns and the subsequent turbulent transport, and possible chemical transformation (e.g. for NOx plumes). But urban emissions enter the urban canopy-layer, where dispersion is often governed by high-rise buildings, and land surface types with various thermal properties. Proper evaluation of the models is important, because the roughness and thermal properties of cities are still poorly resolved at resolutions of ~100m. In WP3-4 we will compare and evaluate three different turbulence resolving models, including the PALM model (Maronga et al., 2020), MicroHH model (Heerwaarden et al., 2017), and the Weather Forecast and Research model (WRF), which can also run in LES mode (WRF-LES; Skamarock et al., 2008).

As a first step in this model intercomparison exercise, we evaluate the sensitivity of the LES models to large scale boundary conditions (meteorological forcings) which includes vertical profiles from re-analysis products combined with local meteorological measurements (Lidar profiles). Different methodologies and assimilation techniques are used to constrain the mesoscale and synoptic conditions, as examined here over Rotterdam and Paris. We present here the uncertainties associated with the meteorological forcings and the impact of various data assimilation (nudging) techniques on the LES model performances.

Table of Contents

Contents

2 Introduction

2.1 Background

The main objectives of WP3 are 1) to define a common protocol for the three LES models (MicroHH, WRF-LES, PALM) over a selection of case studies, 2) to evaluate the impact of large-scale forcing (from the IFS model) on the initial high-resolution model simulations, and 3) to work on the computational efficiency of the LES code to test impact of chemistry and plume rise model in very high resolution simulations of plumes from point sources. The different case studies will be selected among four densely instrumented areas (Paris, Munich, Zurich, and Indianapolis) and one intensive campaign (Rotterdam), all of them including meteorological measurements (e.g. PBL heights and winds) as well as tracer concentrations of CO_2 and NOx (in situ, total column). This work package is a preparation phase for WP4 to define simulation periods, collect evaluation data, and provide the necessary driver data used by the three different LES models: land cover data, building heights, tree canopy, and emissions inventories of fossil fuel CO_2 emissions at high-resolution. High-resolution models highly depend on the large-scale meteorological conditions, provided here by the ERA5 reanalysis fields, in addition to (periodic) turbulence perturbations to generate small-scale turbulence from the boundaries of the domain. WP3 examines the impact of the nudging techniques (spectral, inflow/outflow), and compares the use of intermediate mesoscale domains (nested approach) compared to single-grid and self-nested LES simulations driven by the ERA5 meteorological fields. In addition to urban environments, WP3 will also consider the use of non-CO_2 trace gases such as NOx, as satellite measurements from Sentinel-5p and GEMS missions are already available to infer fossil fuel emissions. However, reactive species such as NOx require the use of non-linear chemistry schemes to simulate the production/destruction rates of NO and NO_2. Due to the additional costs of chemistry schemes, WP3 will develop a GPU-based numerical scheme reducing significantly the computational times. This development will enable the comparison of LES simulations to NO_2 plumes observed by the two satellite missions, while exploring the impact of the chemistry, as currently developed in the CO2MVS system.

There are various challenges to quantify the influence of boundary conditions on simulated trace gases that will be addressed in WP3:

- Critical steps for total column measurements (mass conservation, inflow/outflow, advection of concentrations/fluxes) including
    - Influence of meteorological boundary conditions
    - Coupling methodology (nudging options, open/circular boundary conditions)
- Online (LAM-to-LES) and offline (ERA5-to-LES) coupling:
    - Non-linear NOx chemistry in plumes and plume rise

2.2 Objectives of this deliverable

This deliverable addresses the role of the boundary conditions (BCs) on the simulated concentrations at high resolution. High-resolution models receive lateral, and possibly upper, boundary conditions from the coarser-scale model IFS. This task investigates the impact of spatial and temporal resolution of these BCs on fine-scale simulations, and the impact of the nudging techniques (spectral, inflow/outflow) applied to single or multiple nested domains. Particularly the spatial resolution of IFS model grids and its possible downscaling will be examined. In this task, WUR will conduct MicroHH, URCA WRF-LES and UH PALM simulations for selected case studies.

This deliverable describes sensitivity experiments from two modelling systems over two case studies, eventually intercompared to describe more rigorously the uncertainties associated with high-resolution plume modelling over large cities. The two case studies selected for the intercomparison are Paris (January 2024 – full deployments of Urbisphere and ICOS-Cities projects) and Rotterdam (Sept 2022 - intensive measurement campaign of RITA2022). Both case studies offer a large variety of measurements of greenhouse gasses and meteorological variables (including vertical profiles) taken from mobile and stationary platforms in and around the two cities.

3 Boundary conditions (BCs) on the simulated concentrations at high resolution

3.1 Boundary conditions from ERA5 nudged to wind profiles (MicroHH)

In preparation for the model intercomparison, large-eddy simulations (LES) with MicroHH model were conducted for a domain centred around Rotterdam. The simulations were performed for one day during the RITA2022 campaign (02-09-2022). Figure 1 shows the comparison of the horizontal wind speed and direction measured on the day at three different locations in and around Rotterdam (solid lines). Dotted lines denote the wind simulated by MicroHH (with boundary conditions from ERA5). The differences in the simulated and measured wind speed and direction are obvious. The differences vary per location. The MicroHH wind shows generally similar behaviour between the locations while the measured wind shows more variation. This is likely due to local influences (such as obstacles, local circulations) which remain unresolved in the simulation. Another possible source of mismatch might stem from the fact that the wind in the simulations is forced (nudging, see below) towards ERA5 wind profiles. Although the profiles have decent resolution in time, they are spatially averaged over the whole domain, which might dampen possible local influences on the mean wind.

To try and tackle this issue, we conducted a series of six MicroHH LES runs with the goal of testing the models' sensitivity to the boundary conditions. More specifically, we focus in this report on the wind forcing and the wind drag created by obstacles in the area. To this end, we used vertically resolved measurements of wind speed to create nudging profiles to circumvent the problem of ERA5 not resolving local influences. We also increased the drag coefficient that represents the influence of buildings on the wind.

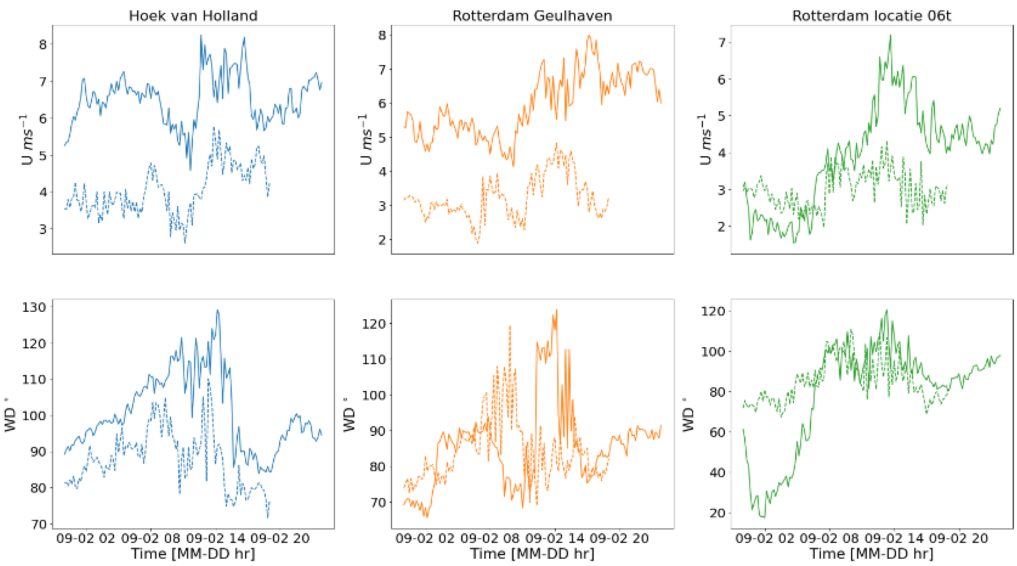

Figure 1 Ten-minute averaged horizontal wind speed (top row) and wind direction (bottom row) obtained from measurements (solid line) and MicroHH simulations (dotted line). The data is obtained at three different locations (columns) on 02-09-2022 at 10 m height. For locations, see Figure 16.

3.2 Boundary conditions from ERA5 in a nested-domain configuration (WRF-LES)

The WRF boundary conditions are nudged to the coarse-resolution domain (D01) while the other domains are forced by their corresponding parent domain (e.g. D01 forcing D02). In addition, we use the Four-Dimensional Data Assimilation scheme (FDDA) to nudge meteorological observations online, as described in the methods section. We present here the model performances over 10 days of simulation (10 to 20 January 2024) for D03 (900m resolution). Two different sets of boundary conditions were coupled to WRF (ERA5 and GFS), both at 0.25 degree resolution. Figure 2 WRF-met-results shows the WRF model performances forced by both reanalysis products regarding temperature, wind speed, and relative humidity. While we assimilated the WMO meteo stations within our FDDA scheme, we utilized the meteorological data from the IOT weather stations network (around 80 stations over D03), available from the AERIS data portal (https://www.aeris-data.fr/) to evaluate the model performances using independent measurements. This dataset differs from the WMO stations, hence providing an independent evaluation of the WRF model performances.

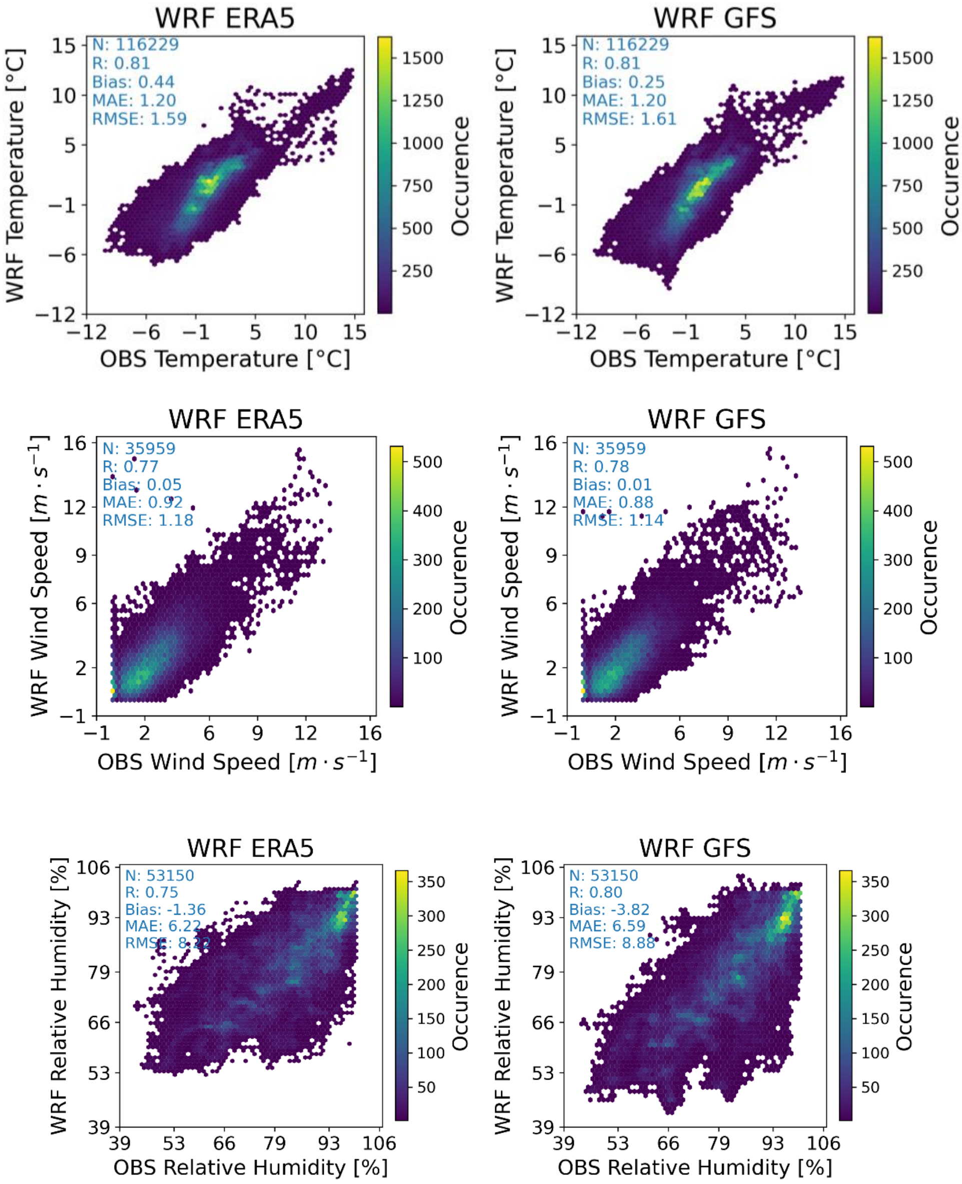

Figure 2 WRF-met-results

The impact of the boundary conditions (ERA5 vs GFS) has a minor impact on our simulation results. GFS introduces a slightly larger bias in relative humidity (-3.8%) compared to ERA5 (-1.4%). The FDDA scheme is responsible for the similarities in model performances, as shown in Deng et al. (2017) thanks to the large number of meteorological measurements available over the region.

We further evaluated the WRF results in terms of wind direction, a critical variable when considering isolated urban plumes. Figure 3 WRF-WindRose illustrated the typical model performances at the Orly airport station. On average, the RMSE in wind direction across stations is about 20-30 degrees at the hourly time step.

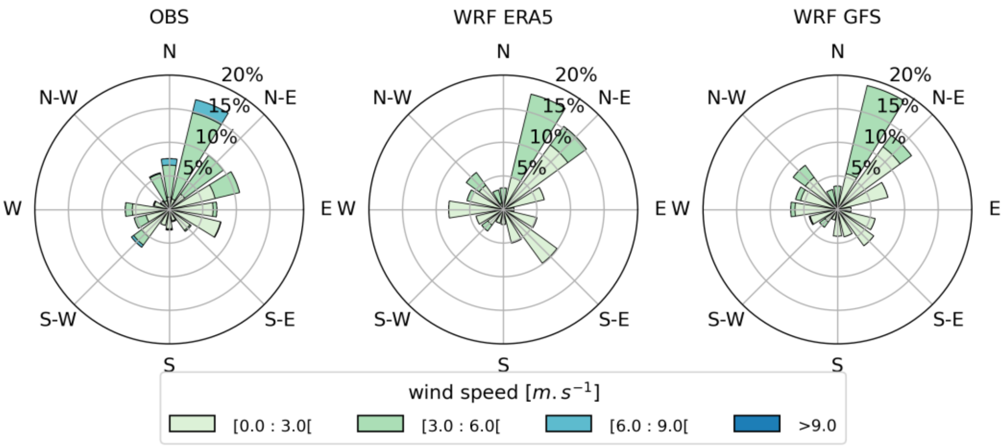

Figure 3 WRF-WindRose: Wind roses simulated by WRF and observed at the Orly Airport station (South of Paris) during the 10 days of simulation.

Considering the mean errors (bias) in wind direction, the WRF model agrees within -3 to +6 degrees depending on the altitude (between 0 to 800m agl) as shown in Figure 4 WRF-WindMBE. The maximum differences between the two boundary conditions reach 2.5 degrees between 250m and 600m agl. This small difference has a minor impact on local CO2 plumes but can generate larger differences over long distances, as illustrated later with XCO2 concentrations at Jussieu (downtown Paris).

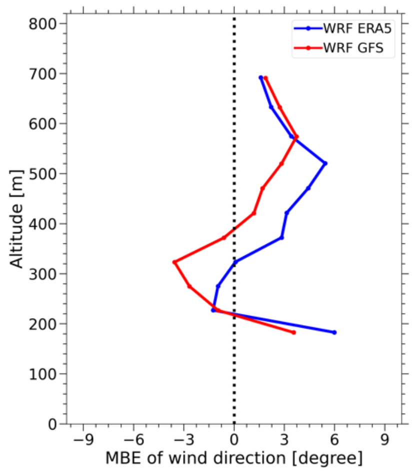

Figure 4 WRF-WindMBE: Mean wind direction error (MBE, in m/s) between WRF and Jussieu Lidar observations during the 10 days of simulation.

3.3 Evaluation of wind profiles (Lidar profilers, WRF-LES)

As we excluded the wind profile data from lidars in our FDDA simulation, we also compared the modelled wind speed at various altitudes (from 0 to 800m agl) to the mean observed wind speeds at three locations (PAARBO, PACHEM, and PALUPD). Figure 5 WRF-Lidar shows the small differences between WRF-LES simulations driven by ERA5 and by GFS, systematically under 0.3m/s even at higher altitudes.

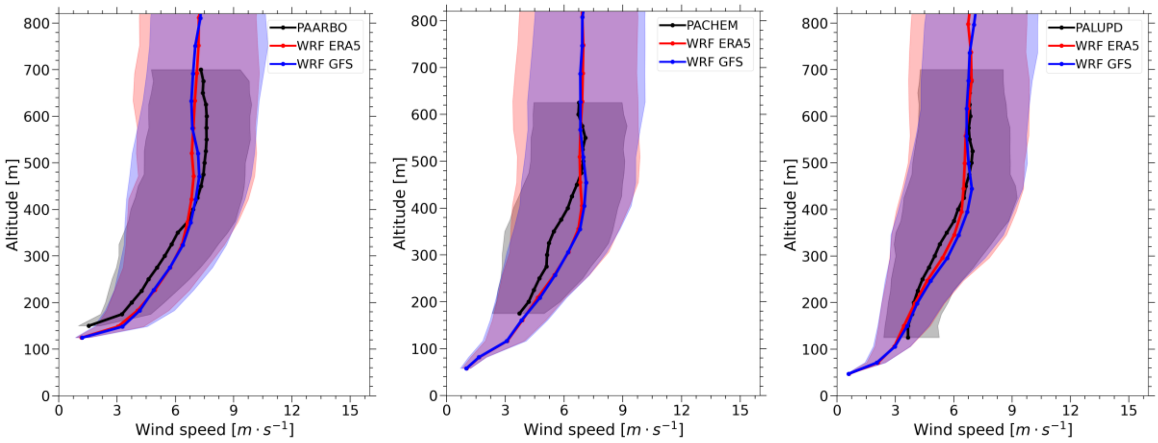

Figure 5 WRF-Lidar: Mean wind speed profiles and their associated standard devations from the WRF model simulation (900m resolution) and observed at three different locations (from left to right: PAARBO, PACHEM and PALUPD) by wind lidar instruments over the period 10-20 January 2024.

3.4 Nudging of wind profiles and Building drag (MicroHH)

As described in the Wind nudging section, wind in MicroHH simulations is forced with horizontally averaged vertical profile of the ERA5 data. However, ERA5 is the reanalysis product with a horizontal resolution of 25x25 km. With that resolution all local influences (such as buildings) on the wind are lost. Therefore, to try and bridge the gap between the simulations and the measurements, the wind has been nudged towards the measurements of the two vertical profiles of the horizontal wind available in the domain: wind lidar and WindCube.

Due to the limited height extend of the data, the two datasets had to be supplemented with ERA5 data to have wind profiles throughout the height of the simulation domain.

Figure 6 (2 left panels) shows the combination of wind lidar measurements up to 240 m and ERA5 profiles that were used above. The wind lidar data was averaged to 1 hour frequency of ERA5 data and linearly interpolated to MicroHH grid. From 240 m to the top of the domain, ERA5 data profiles were used. To avoid sharp gradients on the interface of the two datasets, a one-dimensional Gaussian filter was applied, with σ = 0.5 m/s. It is clear from Fig 6 that the lidar data extends to less than 10 % of the domain.

Similarly, the rightmost panels in Figure 6 show the WindCube data that was supplemented with ERA5 at the bottom and top of the domain. Also for this dataset a 1D Gaussian filter with σ = 0.5 m/s was applied.

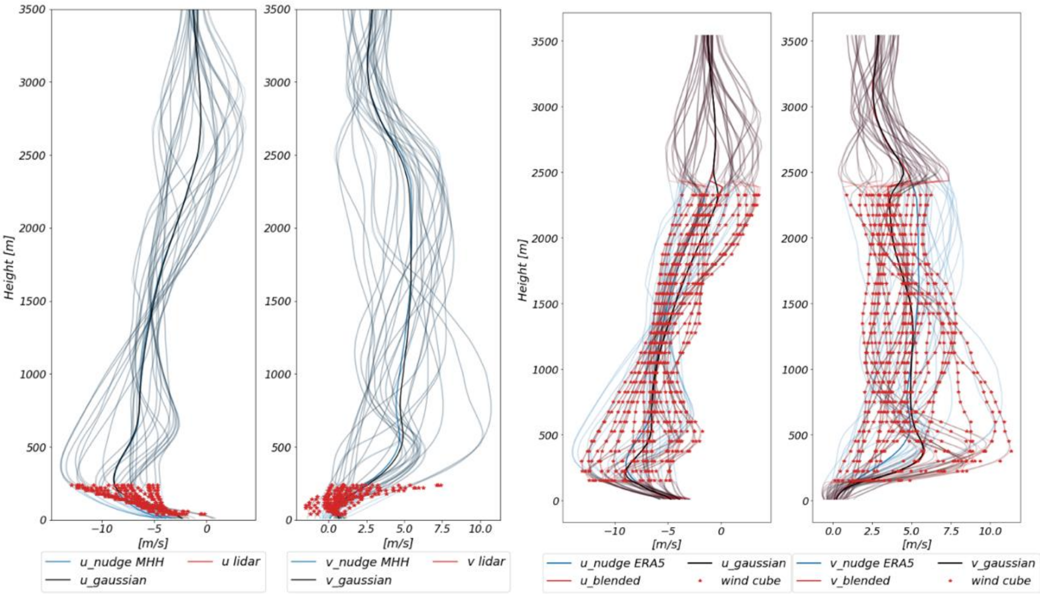

Figure 6 Nudging profiles of u and v wind components used in sensitivity runs. Blue lines in all panels denote standard nudging profiles derived from ERA5. Two left panels show wind components for the runs where wind lidar measurements (red dots) where incorporated with ERA5 wind where lidar data was missing (above 240 m) into new nudging profiles (denoted with _gaussian, black lines). Similarly, the two right panels show WindCube measurements (red dots) filled in with ERA5 wind (blue lines) to create new nudging profiles (black lines).

In order to test the influence of building drag on the wind in simulations we performed simulations in which we varied the bulk drag coefficient c_d (eq. 3). The new coefficients we chose following the paper of Zhang et al (2025) who conducted a series of RANS experiments with different building configurations and from which they calculated the volumetric drag coefficients. We chose three values corresponding to (Zhang et al, 2025, Table 3): medium dense city with varying building heights and (1) rectangle buildings aligned behind each other in streets c_d = 0.64, (2) rectangle buildings staggered behind each other in streets c_d = 0.84. We also chose a configuration for (3) dense city with staggered rectangle buildings c_d = 5.82.

To investigate the influence of the nudging and the building drag on the simulated wind fields, we have set up a series of six experiments in which we simulated one measurement day during RITA2022 campaign. All six simulations had identical set-up varying only bulk drag coefficient c_d or nudging u and v wind profiles. These latter were either derived from ERA5 or as a combination of WindCube measurements at Cabauw and ERA5 or wind lidar at Rotterdam centre and ERA5 as described in the above sections. Table 1 provides an overview of the common specifications of all 6 runs. The run named *ERA5* is used as a reference run. The simulated wind in Figure 1 has been obtained from the ERA5 run, and we will investigate whether the different approaches lead to a better comparison to observations. Table 2 gives an overview of forcings used in the experiments.

Table 1 Common specifications of the 6 LES over Rotterdam.

Domain center (lat lon)	Domain size (x,y,z, km)	Grid size (x,y,z)	Time period
(51.91,4.39)	76.8x76.8x3.5	(768,768,96)	00:00 02-09-2022 – 00:00 03-09-2022

Table 2 Specifications of the origin of the nudging profiles and the bulk drag coefficient in the 6 runs.

Name	Drag coefficient	Nudging
ERA5	0.525	ERA5
Cabauw	0.525	WIndCube+ERA5
Lidar	0.525	Lidar+ERA5
cd064	0.64	ERA5
cd084	0.84	ERA5
cd582	5.82	ERA5

3.5 Impact of the nudged boundary conditions (MicroHH)

Figure 7 shows domain averaged vertical profiles of u and v as mean over the whole 24-hour simulation. As expected, for most runs wind speed profiles fall on the same line because higher in the domain they are all nudged towards ERA5 profiles. The only exception is the Cabauw run which was nudged towards WindCube measurements from 150 to 2400 m height. Close to the ground the values of the u wind component differ, as there the influence of building drag and wind lidar are felt. The lack of differences in the v wind is expected as the mean wind is predominantly easterly, and the v component is small.

Figures 8-11 depict the *differences* between wind measurements and the simulated winds in the 6 runs. To this end, 10-minute averages of wind speed and direction from the simulations were subtracted from the 10-minute averages of the three KNMI stations. To show the diurnal variations, these were then aggregated into 4-hour bins to create box plots (Figs. 9–11). In Figure 8 the difference between the simulations and the wind lidar is shown. These differ from Figs 9–11 in that the differences in wind speed and direction are also averaged over height. These differences were calculated for all available measurements (up to 240 m, for each time step) and then first averaged over height before aggregating them into 4 hour intervals.

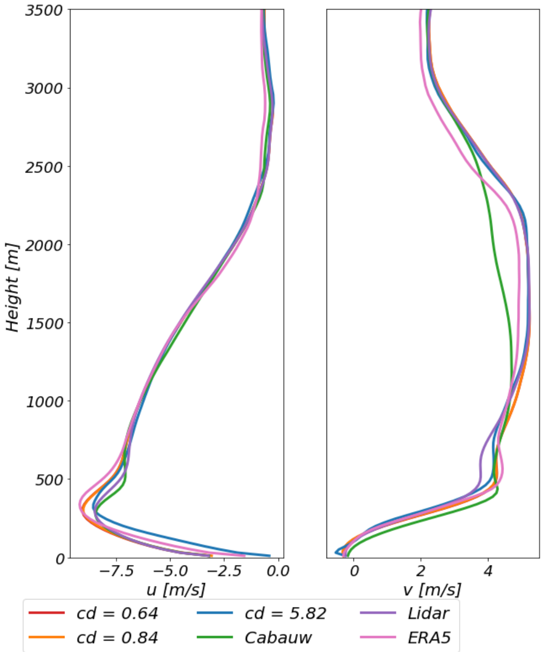

Figure 7 Horizontally (domain) averaged and time averaged (the whole simulation) u and v wind speeds from all 6 runs.

In analysing the results, none of the 6 runs show a clear improvement in their agreement with observations. The differences in wind speed and direction vary from location to location in their magnitude and sign. In rare instances (Rotterdam, 6am local time) the MicroHH wind is too strong in comparison to observations, but generally the wind in MicroHH is too slow, with substantial variation across all simulations. This could be a local effect that is not captured with the ERA5 resolution and which is not visible in the 2 wind sensitivity simulations because (1) lidar measurements extend only to 240 m height and are overpowered by the mixing with the wind above, which is still nudged towards ERA5, and (2) the WindCube at Cabauw is too far away to accurately represent local influences in Rotterdam. One general observation that can be made in all figures is the influence of the very high prescribed drag (cd = 5.82) on wind speed. This is noticeable in all locations, but especially at Hoek van Holland, which is located at the coast and close to the harbour where the surroundings are not expected to resemble a dense city. Conversely, in Geulhaven (Fig. 9), which is in the city, the influence is less noticeable.

Differences in wind direction are not as consistent as with wind speed. Here the variation in differences between the simulations and measurements is more prominent. For example, the observations completely miss the wind turning at Rotterdam locatie 06 in the early morning during very low wind speeds (Fig. 11), as well as sudden wind direction changes (wind speed quite consistent) during the 12 – 16 pm period at Rotterdam Geulhaven (Fig. 9). Conversely, the wind direction differences between simulation and observations at Rotterdam centre (Fig. 8) stay consistently small throughout all simulations.

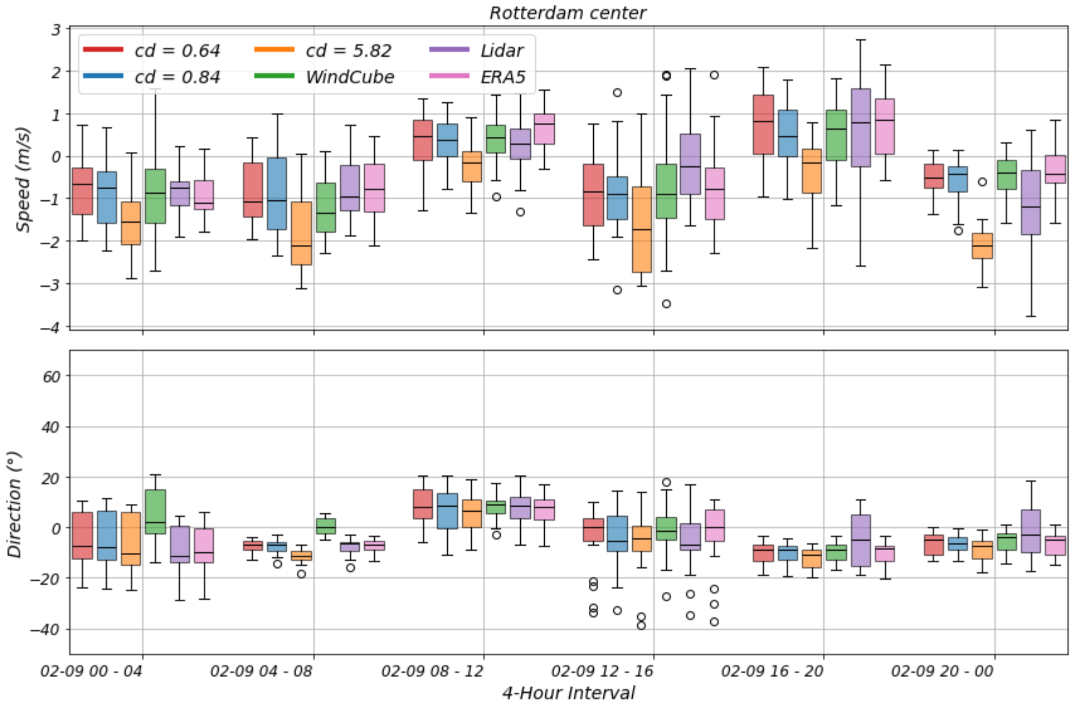

Figure 8 Wind speed (top) and direction (bottom) differences (simulations - measurements) for the 6 simulations. The simulations are compared to the point wind lidar measurements at Rotterdam centre. Boxplots show interquartile range (IQR), with black line denoting the median, and whiskers showing Q1 – 1.5*IQR (bottom) and Q3 + 1.5*IQR (top).

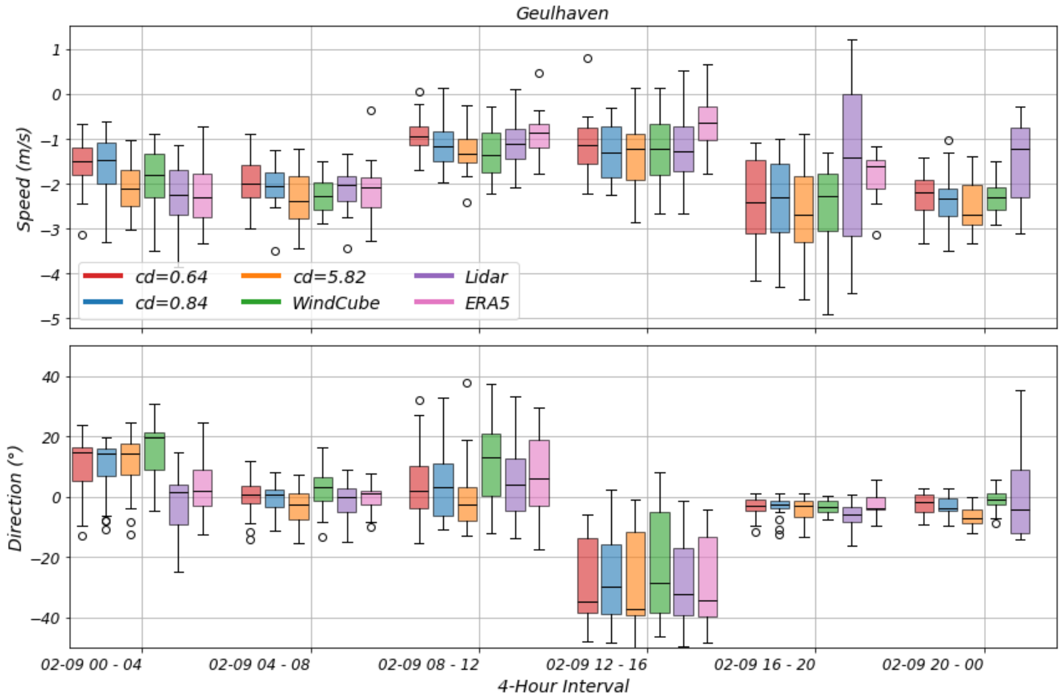

Figure 9 Wind speed (top) and direction (bottom) differences (simulations - measurements) for the 6 simulations. The simulations are compared to the point wind measurements at Rotterdam Geulhaven (west of city center). Boxplots show interquartile range (IQR), with black line denoting the median, and whiskers showing Q1 – 1.5*IQR (bottom) and Q3 + 1.5*IQR (top).

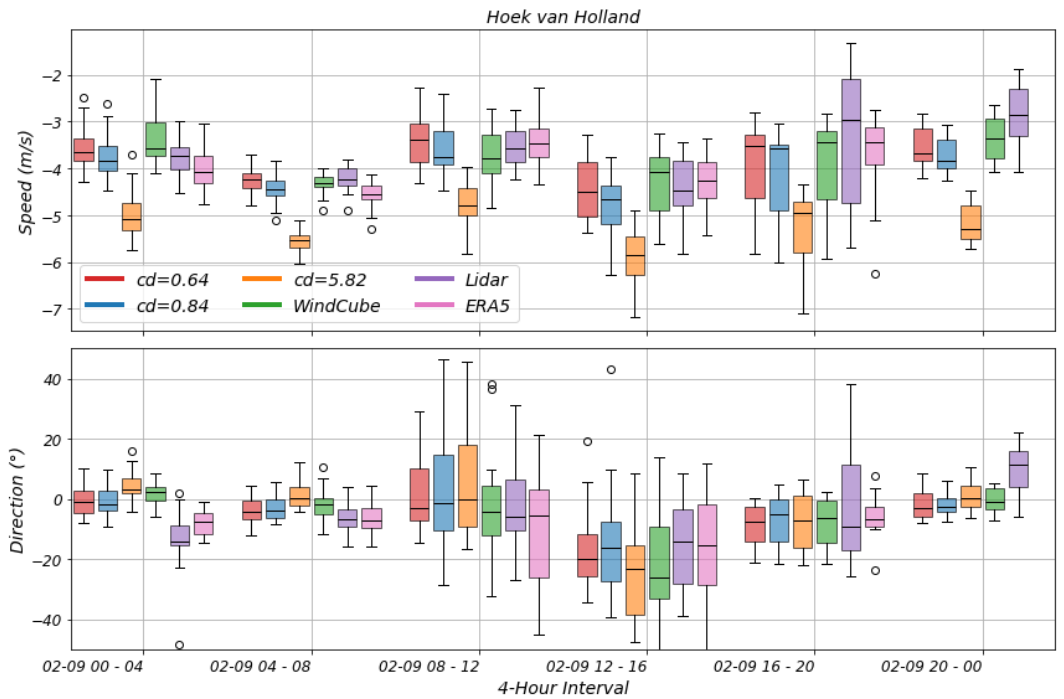

Figure 10 Wind speed (top) and direction (bottom) differences (simulations - measurements) for the 6 simulations. The simulations are compared to the point wind measurements at Hoek van Holland (on the coast, in the harbor). Boxplots show interquartile range (IQR), with black line denoting the median, and whiskers showing Q1 – 1.5*IQR (bottom) and Q3 + 1.5*IQR (top).

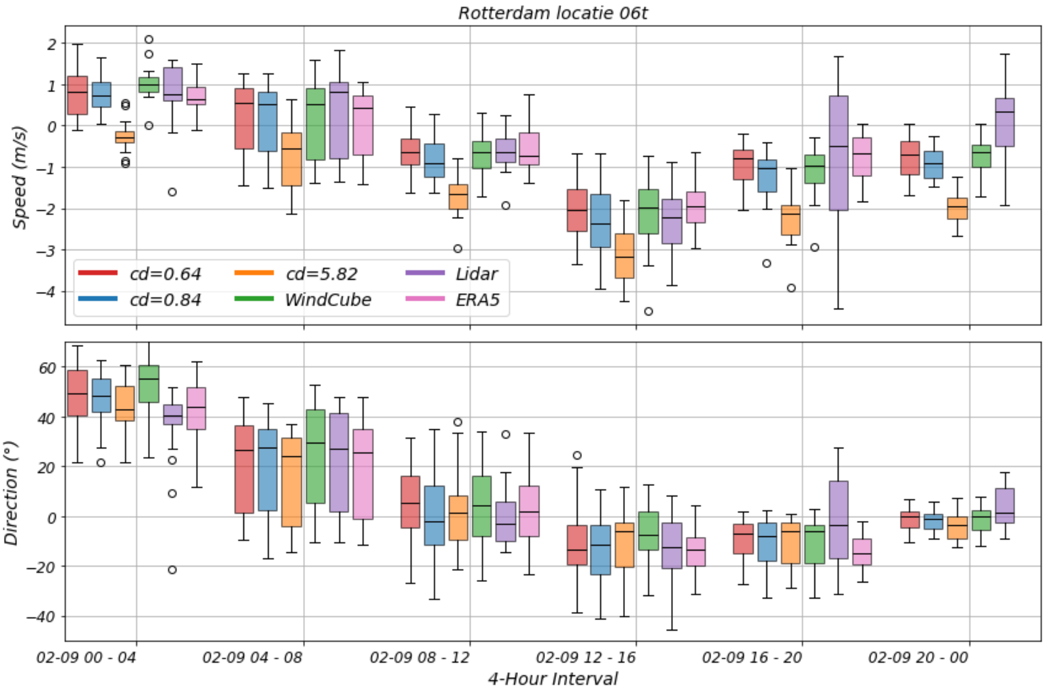

Figure 11 Wind speed (top) and direction (bottom) differences (simulations - measurements) for the 6 simulations. The simulations are compared to the point wind measurements at Rotterdam locatie 06t (airport). Boxplots show interquartile range (IQR), with black line denoting the median, and whiskers showing Q1 – 1.5*IQR (bottom) and Q3 + 1.5*IQR (top).

3.6 Impact on Atmospheric CO_2 concentrations (WRF-Chem)

We evaluate here the impact of the meteorological boundary conditions on the atmospheric CO2 concentrations. Boundary conditions impact both the structure of the urban CO2 plumes and the spatial gradients due to the large-scale CO2 inflow. As illustrated in Figure 12 WRF-CO2Map, the regional CO2 enhancement varies depending on the boundary conditions. The general orientation of the CO2 plumes remains similar, to the exception of small variations in wind speed/direction (e.g. to the North of Paris). The magnitudes of the CO2 enhancements vary as well but remain also similar in both simulations.

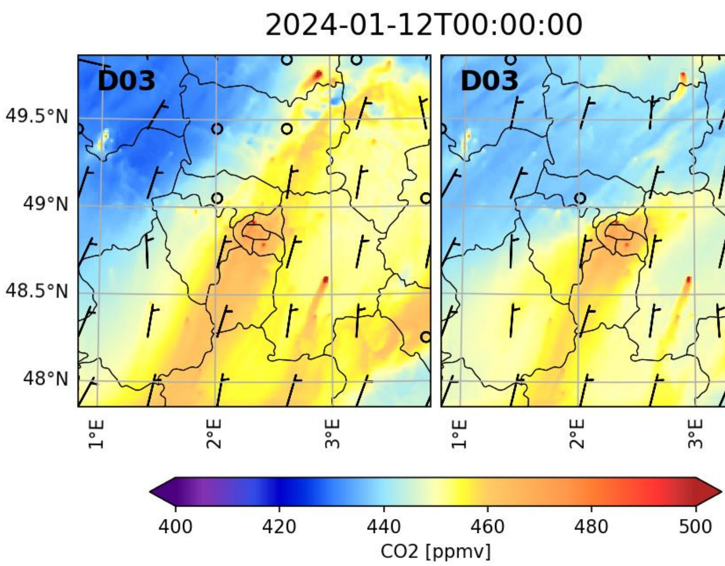

Figure 12 WRF-CO2Map: Atmospheric CO_2 concentrations (in ppmv) modelled by WRF-Chem coupled to ERA5 (left panel) and by GFS (right panel) at the first level of the model (0-20m agl).

We compiled the model statistics using all the available CO2 stations in and around Paris, separating the daytime data typically used in atmospheric inversions (large transport errors at night). Figure 13 WRF-PLACO2 shows the scatter plots at the PLA station using ERA5 and GFS. The overall scores (MAE and RMSE) remain fairly similar using both boundary conditions.

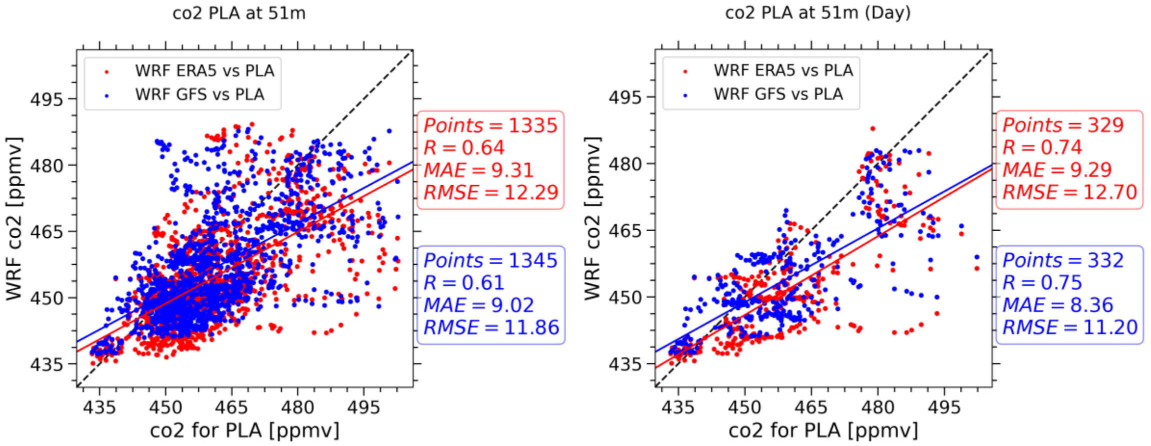

Figure 13 WRF-PLACO2: Atmospheric CO_2 concentrations (in ppmv) modelled by WRF-Chem coupled to ERA5 (in red) and by GFS (in blue) at the PLA station for all times of day (left panel) and only during daytime (right panel).

When considering all the CO_2 stations available during our simulation period (10-20 January 2024), the model performances remain similar with both drivers, while introducing a different bias over 10 days (cf. Figure 14 WRF-AllCO2). The mean error in CO_2 concentrations can introduce a flux bias when performing the CO_2 flux inversion over the Paris area (-8.42ppm for ERA5 and -6.2ppm for GFS). We also examined the origin of the CO_2 differences in the atmospheric columns (Figure 15 WRF-JUS_XCO2, right panel), and noted that this bias remains constant over multiple days. According to the duration of the bias and considering the absence of noticeable biases in wind speed/direction nor temperature, we suspect that the introduction of such a difference in CO_2 concentration is due to long-distance sources, possibly located in D01 or D02. We will investigate this bias when performing backward particle footprints with a Lagrangian model. However, the structure of the urban CO_2 plumes is similar in both simulations, as shown in Figure 15 WRF-JUS_XCO2 (left panels) for the total atmospheric CO_2 columns across D03 (900m resolution).

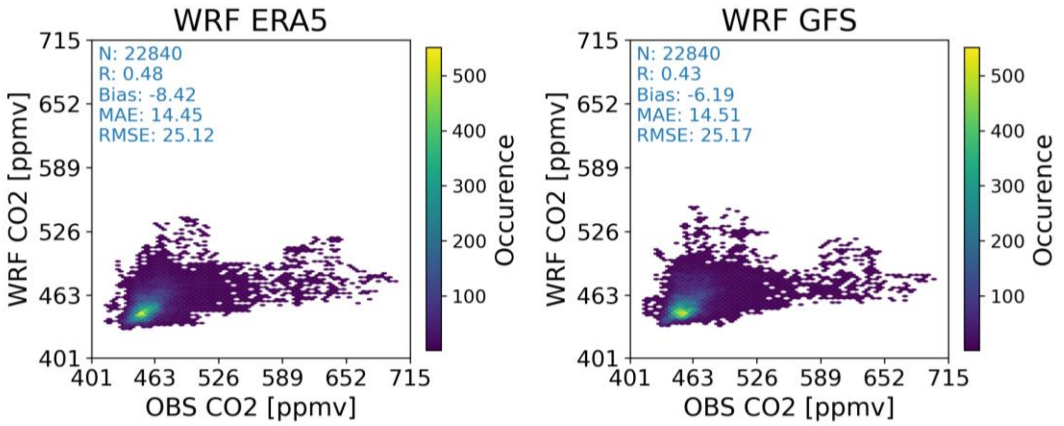

Figure 14 WRF-AllCO2: Atmospheric CO_2 concentrations (in ppmv) modelled by WRF-Chem coupled to ERA5 (left panel) and by GFS (right panel) at all the stations for all times of day.

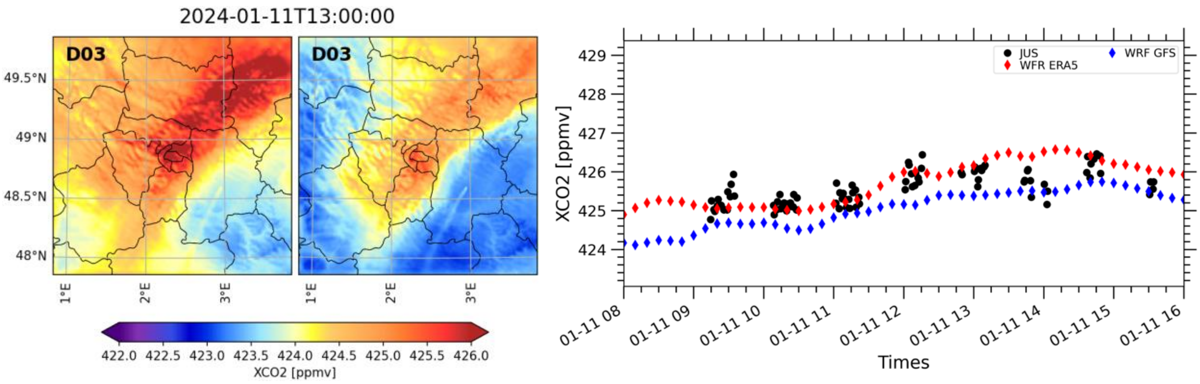

Figure 15 WRF-JUS_XCO2: Maps of total column atmospheric CO_2 concentrations (in ppmv) modelled by WRF-Chem coupled to ERA5 (left panel) and by GFS (middle panel) and time series at the JUS station (TCCON location) from 10 to 20 January 2024 (right panel).

3.7 Deviations and counter measures

The boundary conditions were originally supposed to be extracted from the IFS simulations. As both LES models (MicroHH and WRF-LES) were configured and tested using ERA5, we decided to examine the boundary condition impact using a known and tested configuration instead of producing new model simulations with a new product. As IFS simulations are being made available, we will work on the coupling strategy with the IFS meteorology, modifying existing nudging schemes. As noted here, both models require additional forcing through nudging strategies, hence limiting the impact of the large-scale boundary conditions from reanalysis products. We conclude here that future LES systems need to assimilate local meteorological measurements to achieve sufficient performances.

4 Methods

4.1 MICROHH

MicroHH is a fluid dynamics code designed to perform direct numerical simulations (DNS) and large-eddy simulations (LES) in either idealized theoretical settings or realistic atmosphere (as described in van Heerwaarden et al. (2017)). Realistic atmosphere simulations are achieved by coupling MicroHH with ERA5 reanalysis data (Hersbach et al. 2020) data by using the Large-eddy simulation and Single column model – Large-Scale Dynamics ((LS)²D) Python package developed by van Stratum et al. (2023). MicroHH is capable of simulating both scalar and reactive plumes. The code is freely available on GitHub and can be downloaded following the instructions on the projects' Read the Docs site.

Large-eddy simulations have been implemented in MicroHH using a surface model that has been constrained to rough surfaces and large Reynolds numbers that is representative of typical atmospheric flows. The model solves surface fluxes of momentum and scalar components using the Monin-Obukhov similarity theory (MOST, e.g. Stull, 2012). To solve the sub-grid kinematic momentum flux tensor, MicroHH uses the Smagorinsky-Lily model (Lily, 1996, van Heerwaarden, 2017). Transport of scalars is solved with the advection-diffusion equation. For the reactive species, chemistry in the model is solved using a condensed chemistry scheme which is based on the scheme implemented in the CAMS/IFS system (Inness et al.,2019, Krol et al., 2024).

Plume dispersion from point sources in MicroHH LES has been validated against wind tunnel experiments (Nironi et al., 2015) for a neutral channel flow by Ražnjević et al. (2022)a. It has also been used by Ražnjević et al. (2022)b to simulate methane plume dispersion from a point source in a realistic atmosphere. In that study, a measurement day during a campaign in Romania has been simulated with realistic meteorology boundary conditions. More recently, Krol et al., (2024) have used MicroHH to simulate chemically active NO_x plumes from various large point sources, which were then evaluated against TROPOMI measurements.

4.2 Boundary conditions in MicroHH

To perform MicroHH simulations as close to the true atmospheric conditions as possible, boundary and initial conditions are prescribed from various inventories or from outputs from other models. How these values are prescribed depends on the variable itself. For example, surface conditions, such as the vegetation type or locations of bodies of water remain constant at the lower boundary throughout the simulation. Conversely, the wind profiles are prescribed as initial conditions, after which the wind is left to develop in the simulation with periodic boundary condition (the turbulent lateral outflow from the domain is used as inflow on the opposite boundary). In this process, only the domain-averaged profiles (wind, temperature, moisture) are nudged to the prescribed boundary conditions, so that the simulation does not drift away.

In this text the focus will be on the boundary conditions that affect the wind in the simulations, more specifically, we will look at the influence of the building drag and the nudging profiles on the simulated wind.

4.3 Observations (Rotterdam case study)

During the RITA2022 period several instruments were measuring wind speed and direction in and around Rotterdam. Figure 16 gives an overview of the measurement locations. Four wind instruments, Hoek van Holland, Rotterdam Geulhaven. Rotterdam locatie 06t and 24t are part of the Dutch Royal Meteorological Institute (KNMI) measurement network and are permanently stationed at the indicated locations. Cabauw is a measurement supersite. Finally, the wind lidar was part of the RTA2022 campaign. The following sections give a closer look to the measurements on the chosen simulation day.

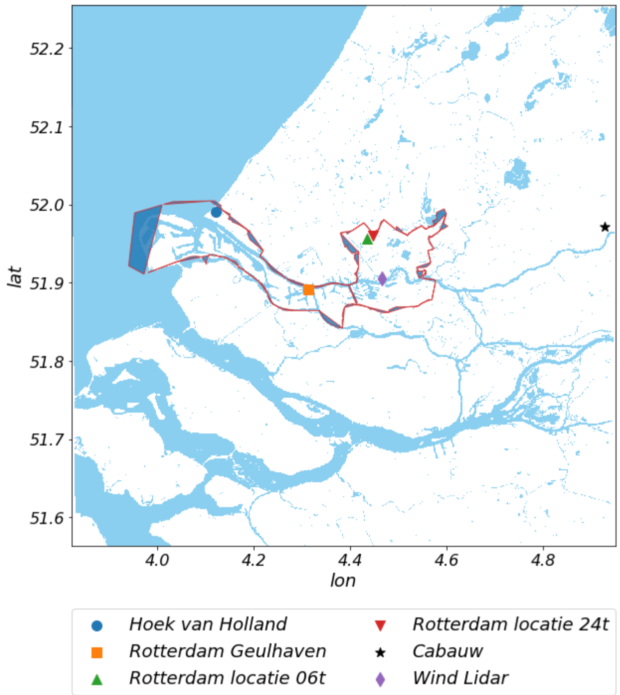

Figure 16 Overview of locations where wind measurements were taken during RITA2022.

4.3.1 WindCube measurements at Cabauw

The Cabauw tall tower supersite is located between the cities Rotterdam and Utrecht in an area characterized by grassland and farmland. It is located at the coordinates (51.971° N, 4.927° E). Among the instruments at the site there is a WindCube which measures 10 min averages of horizontal wind speed and direction. The measurements are taken at vertical levels with 75 m resolution starting from 150 m and extending above the top of the troposphere (to approx. 14 km). However, due to data quality considerations, only the measurements up to 2400 m were considered in this work. Wind direction (Figure 17, lower panel) is approximately consistent throughout the day (100 -150 degrees), with only notable wind turning above 1500 m after sunset. Wind speed shows low-level jets during both nights with peak winds of 14 m/s at about 250 m height. During the day, horizontal wind is approximately uniform up to about 2000 m indicating the top of the boundary layer.

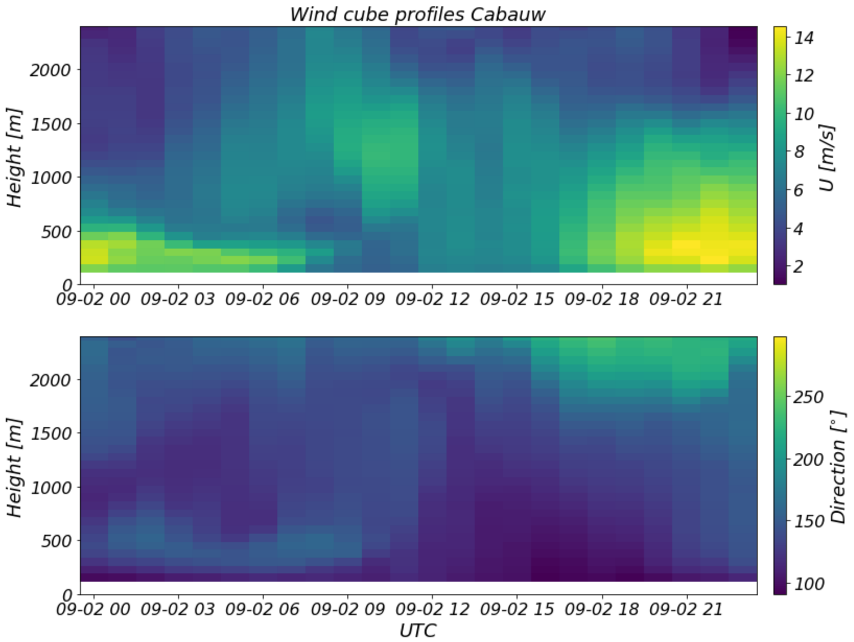

Figure 17 Measurements of 10 minute averages of horizontal wind speed (top) and direction (bottom) taken at Cabauw on 02-09-2022. Measurements were taken with a WindCube.

4.3.2 Wind lidar measurements at Rotterdam Center

During the RITA2022 campaign a wind lidar instrument was placed in the city centre of Rotterdam at the coordinates (51.9258°N, 4.4661°E). The instrument measured 10-minute averages of horizontal wind speed (WS) and direction (WD) at altitudes from 40 m to 240 m with 20 m vertical resolution. Figure 18 shows the measurements of the wind lidar for the chosen simulation day. From the bottom subplot it is visible that the wind direction remained approximately constant at about 100 degrees throughout the simulations period. For Rotterdam this means that easterly winds were blowing from inland to the sea. Noteworthy is the noise in the WD at the surface from midnight until 3 AM. We speculate this is due to the very low wind conditions (< 2 m/s) during the night in the stable boundary layer. Like the WindCube data in Fig. 17, we observe the development of low level jets at night with wind speeds of about 14 m/s.

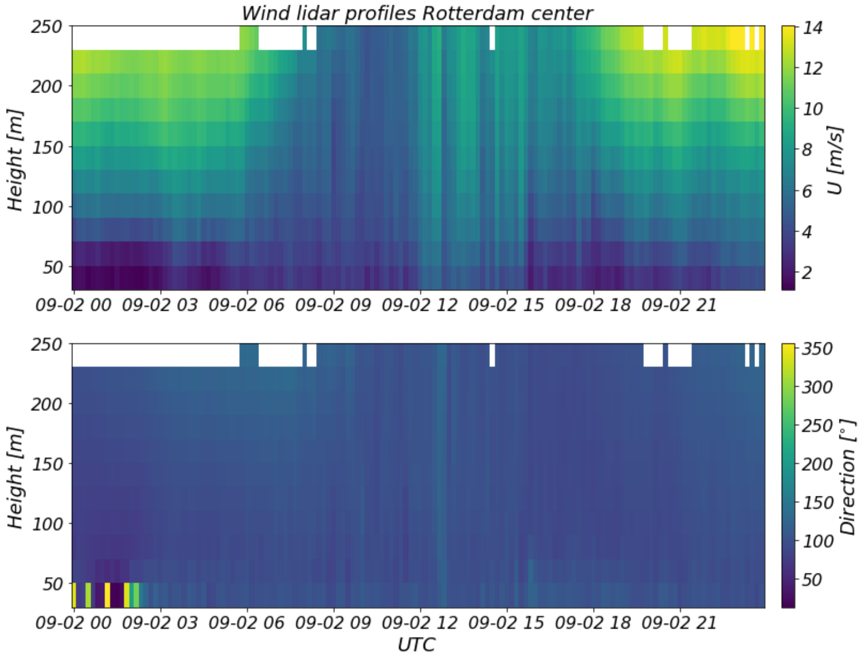

Figure 18 Measurements of 10-minute averages of horizontal wind speed (top) and direction (bottom) taken at Rotterdam city centre on 02-09-2022. Measurements were taken by a wind lidar.

4.3.3 Surface meteorological measurements (KNMI stations)

Unlike wind lidar and WindCube, measurements at KNMI stations are point measurements taken at 10 m above the ground represent 10-minute averages of horizontal wind speed and direction. Figure 19 shows the measurements at three locations indicated in Figure 16. All three locations differ in the measured wind speed and direction apart from the periods with a fully developed planetary boundary layer (PBL) (approx. 12 – 16 pm). The measurements at two locations next to the river (Hoek van Holland and Geulhaven) show more similar behaviour with each other than with the measurements at the third location (Rotterdam locatie 06t). Rotterdam locatie 06t is close to Rotterdam Airport, which is located more inland. There, notably, during the first night the windspeed is much slower and the direction is quite different from the wind direction at the other stations.

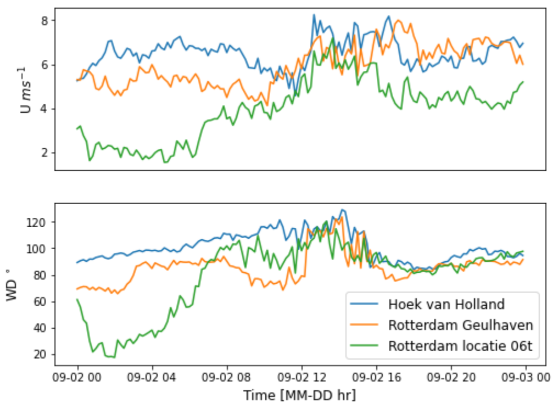

Figure 19: Ten-minute averages of horizontal wind speed and direction at three locations in and around Rotterdam. Measurements were taken at 10 m height.

4.4 Wind nudging in MicroHH

As mentioned above, in MicroHH simulations turbulence develops freely governed by the influence of the surface roughness (that affects the wind profile) and surface heat and moisture fluxes. While it is desirable that the turbulence develops unhindered, the mean wind profiles should correspond to the actual field conditions as close as possible. In MicroHH this is ensured by nudging the horizontally averaged wind towards some reference value. Historically, the simulations are nudged towards the ERA5 reanalysis data (e.g. Ražnjević et al. (2022)b), but they can be nudged towards any vertical profile. ERA5 profiles that are used for nudging are obtained by taking hourly ERA5 fields that have been averaged over the simulation domain. This results in referent vertical profiles ($X_{ref}(z)$) of relevant variables towards which the simulation is then adjusted. The nudging is then performed by adding a forcing term to the tendency equation. As an example we give the equation for the u wind component (eq. 1)

$$\frac{\partial u}{\partial t} = LES\ Dynamics + N. \tag{1}$$

Here the LES Dynamics is a blanket term for all other components of this equation that are out of scope for this work. N is the nudging term. The nudging term is calculated in every time step using the equation 2:

$$N = -\lambda(z)\left(X_{avg}(z) - X_{ref}(z)\right). \tag{2}$$

Here, $X_{ref}(z)$ is the above-mentioned reference profile, $X_{avg}(z)$ is the horizontal average of the relevant variable (in this example u wind) and $\lambda(z)$ is the relaxation factor that corresponds to frequency of nudging and governs how strongly the simulation is being steered towards the reference profile. If the timescale of nudging is very small ($\lambda(z)$ large) then the simulation does not have the chance to develop freely and $X_{avg}(z)$ will be strongly forced to $X_{ref}(z)$. In MicroHH this factor is small enough that the turbulence has the chance to develop, but large enough that the drift from the reference profile is not big.

4.5 Building drag in MicroHH

MicroHH does not support solid objects in the LES domain. For domains in which canopy has significant influence on the simulated wind, such as forests or cities, drag can be parametrized with a drag force term D. The drag force is defined as:

$$D = -\rho_b c_d |U| u_i \tag{3}$$

Where c_d is the drag coefficient, a dimensionless number which depends on the shape and arrangement of buildings, |U| is the wind speed, u_i is the three dimensional velocity in the i = [i, j, k] direction and ρ_b is the building area density, which in MicroHH is defined per grid point as

$$\rho_b = \frac{A_b}{V} = \frac{(DV)^{\frac{2}{3}}}{V} \tag{4}$$

Here, D is a volume fraction that a building occupies within one grid box, V = dxdydz is the volume of one grid box. For Rotterdam, these are derived from available high-resolution height maps (AHN, https://www.ahn.nl/dataroom). Finally, as with the nudging term, the drag force is imposed on the flow through the tendency equation

$$\frac{\partial u}{\partial t} = LES\ Dynamics + D \qquad (5)$$

Where the left-hand side and LES Dynamics term have the same meaning as in eq. 1. Note that the drag is applied to all three wind components.

4.6 WRF-LES model description

The Weather Research and Forecasting (WRF) model (Skamarock et al, 2008, 2019, https://github.com/wrf-model/WRF) is a widely used numerical weather prediction and atmospheric simulation tool, designed to address a range of meteorological and environmental studies. WRF's high-resolution capabilities, robust physics parameterizations, and flexibility make it a critical component for urban greenhouse gas (GHG) emission simulations. The WRF model has been widely utilized in numerous studies investigating greenhouse gas (GHG) emissions, demonstrating its significant potential to accurately simulate GHG concentrations and their spatial-temporal distribution. Its ability to incorporate detailed atmospheric processes and fine-scale spatial resolutions allows for a comprehensive understanding of emission sources and transport mechanisms of GHGs. Previous studies have shown that the WRF model is particularly effective in simulating the dispersion of GHGs at regional scales (Lauvaux T., et al. 2016; Gaudet, et al., 2017; Matthäus Kiel et al., 2021; Chulakadabba et al. 2023; Alexandre Danjou et al., 2024).

The Large Eddy Simulation (LES) mode in WRF is designed for high-resolution simulations with grid spacings << 1 km, explicitly resolving turbulence and eddies at fine scales. LES is particularly effective for grid resolutions up to about 100 m. This resolution is crucial for simulating the complex turbulence structures and flows in environments such as urban areas. While WRF Planetary Boundary Layer (PBL) schemes are suited for grid resolutions greater than 1 km, LES explicitly resolves the major eddies, enabling 3-D turbulence schemes to handle sub-grid mixing. This allows LES to capture critical processes in urban settings, such as tracer (CO_2 or CH_4, …) dispersion, influenced by buildings and streets, urban heat islands, and complex urban flows. However, the grid spacings between 200 m and 1 km is considered as a grey zone, where neither PBL and LES assumptions are perfect.

4.7 Boundary conditions, nesting configuration and nudging

The WRF-Chem boundary conditions are extracted from the ERA5 (hourly, 0.25° x 0.25°, ECMWF) and GFS (3-hourly, 0.25° x 0.25°, NCAR) meteorological fields to constrain the large-scale conditions on the edges of the largest domain (Domain 1, or D01). The nudging technique has been described in numerous studies, here nudged with a linear coefficient over five pixels along the edges of the parent domain (e.g. Lauvaux et al., 2012; Deng et al., 2017). The nesting configuration includes five domains with a nesting coefficient of three, starting at 8.1km down to 100m resolution (for domain 5). Figure 20 Nesting shows the spatial extent of the five domains, using mesoscale physics (domains 1 to 3) and LES mode (domains 4 and 5). On the right panel, the atmospheric CO_2 stations are represented by red dots while meteorological wind lidars are shown in blue.

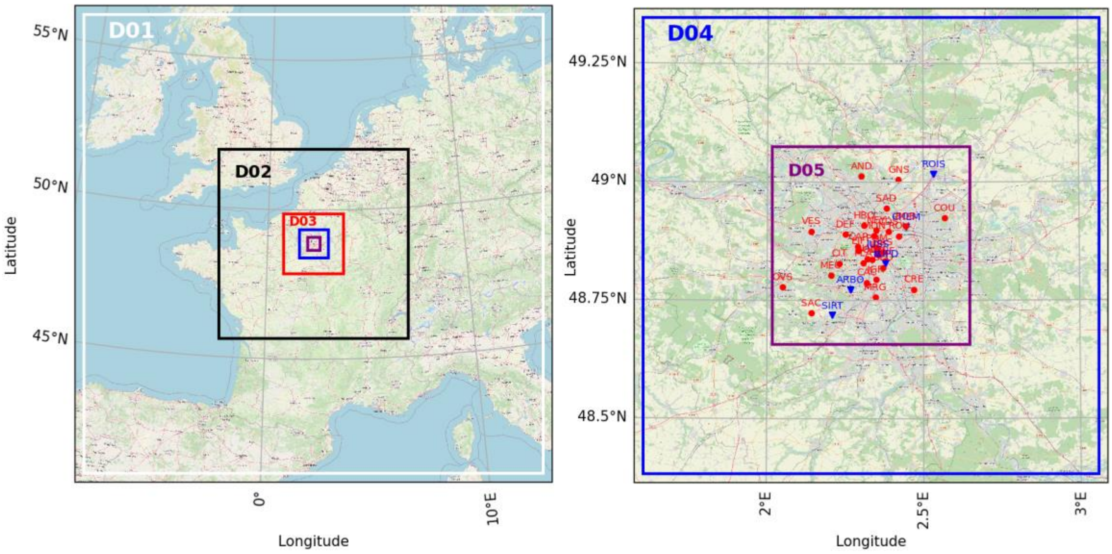

Figure 20 Nesting: Simulations domains used for WRF simulations in nesting mode including the three mesoscale mode (D01, D02, D03) and in LES mode (D04 and D05), including atmospheric CO2 sensors (red dots) and wind lidars (blue dots) used for the model evaluation

To improve the performances of the WRF simulations, the WRF model was run using the FDDA scheme (nudging) with meteorological measurements collected and QA/QC by the World Meteorological Organization (WMO). Figure 21 NudgeData shows the locations of surface stations (red triangles) and upper-air data (blue triangles, incl. rawinsondes and aircraft data) assimilated online with domains 1 to 3 (mesoscale mode). No FDDA scheme was used in LES mode to avoid numerical instabilities with the explicit turbulence. Overall, we assimilated 11 stations over domain 3 (900m resolution), 157 stations over domain 2 (2.7km) and 934 stations over domain 1 (8.1km), every 3 hours.

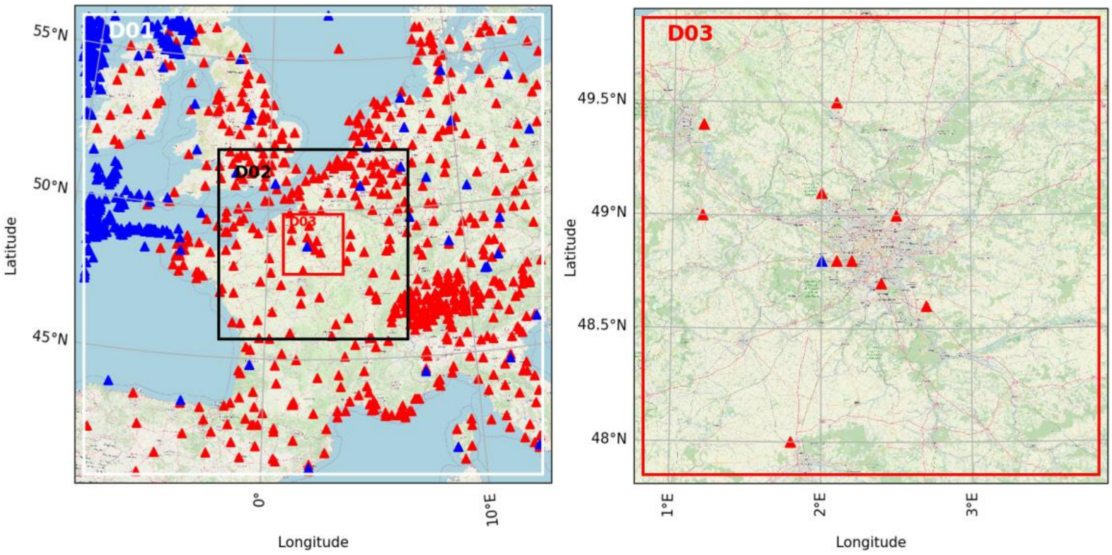

Figure 21 NudgeData: Meteorological measurement locations assimilated in WRF (FDDA scheme) including WMO surface stations (red triangles) and upper-air data (blue triangles) from rawinsondes and aircraft.

4.8 Surface CO2 fluxes, emissions and CO_2 boundary inflow

WRF-GHG (Beck et al., 2012) in the WRF-Chem model simulates CO_2 as a passive tracer, focusing on transport and mixing without chemistry or removal processes. Each surface flux component (biogenic, fossil fuel, boundary inflow) can be categorized into separate tracers, allowing for the attribution of various sources and sinks during a single simulation.

The biogenic fluxes are simulated with the Vegetation Photosynthesis and Respiration Model (VPRM) (Mahadevan et al., 2008). VPRM has been run offline driven by ERA5 meteorological and surface conditions, including MODIS data and high-resolution land surface maps (CORINE). VPRM uses MODIS data, such as Enhanced Vegetation Index (EVI) and Land Surface Water Index (LSWI), along with meteorological parameters from ERA5, to model photosynthesis and respiration processes. The simulated biogenic CO_2 surface fluxes from VPRM are coupled to WRF to simulate the biospheric contribution in the atmospheric CO_2 concentrations. This allows the inclusion of natural CO_2 fluxes in simulations alongside anthropogenic sources.

The fossil fuel contribution is modelled using a high-resolution inventory produced by the local air quality agency of Paris (AirParif) describing each sector of the human activities at 500m resolution for each hour of the year. This product has been developed during the ICOS-Cities project (funded by Horizon Europe) following previous versions utilized in inversion studies over Paris (e.g. Staufer et al., 2015). To simulate the transport and dispersion of tracers accurately, WRF integrates real-world boundary data from global models (e.g., CAMS) to ensure realistic lateral boundary conditions, as in Lian et al. (2022).

4.9 Meteorological and CO2 observations over Paris

The atmospheric measurements used in this study have been described in the simulation protocol (D3.1) and are only summarized here for the evaluation of the WRF model performances. During the URBISPHERE project, 6 stations were deployed across Paris and Île-de-France to measure vertical profiles of wind speed and directions (Figure 22 Lidar).

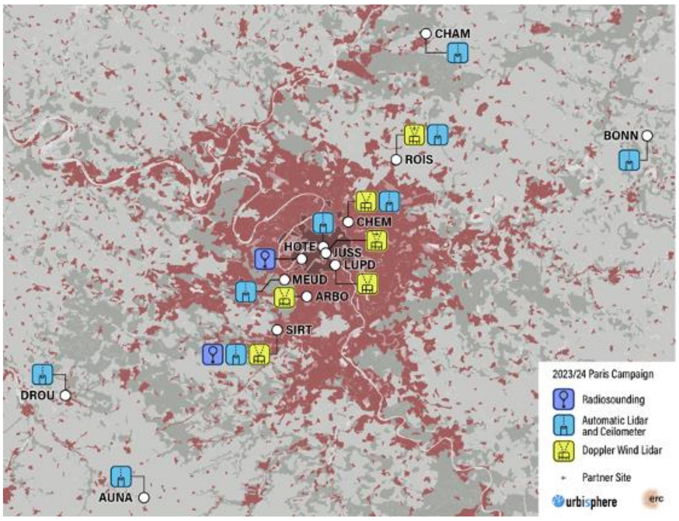

Figure 22 Lidar: Map of the deployed Doppler Wind Lidars and Ceilometers during the selected period as part of the Urbisphere project (courtesy of A. Christen, Univ. Of Freiburg)

Total Carbon Column Observing Network (TCCON): the station is in the centre of Paris, at Sorbonne Université, Campus Pierre et Marie Curie, 4 Place Jussieu, Paris 05, France (48.85 N, 2.36 E). Data in netCDF format are publicly available (http://tccon.org/).

EM27: Currently we have access to data from two EM27 stations, located at Gonesse (48.991°N, 2.445°E) and Saclay (48.711°N, 2.148°E).

Paris Mid-cost CO_2 sensor network: As part of the ICOS-Cities project, a network of **over 25 mid-cost CO_2 sensors** has been strategically installed throughout the urban and suburban areas of Paris.

4.10 PALM model and dynamic driver

PALM model system can be used with a dynamic driver for input data updated at regular intervals from a coarser mesoscale model, in this case from WRF [Kadasch et. al. 2021]. The input data must include the three-dimensional wind components u, v, w, potential temperature and specific humidity. Additionally, PALM has multiple modes in its radiation module for including incoming shortwave and longwave radiation. In the PALM simulations an external mode is used, where spatially averaged 1D temporal evolution of SW and LW radiation are also calculated from WRF [Maronga et. al. 2020].

PALM is supplied with a set of scripts called WRF interface, which is a tool developed by PALM developers to prepare WRF output to a dynamic driver [Vogel et. al. 2022]. The tool handles regridding, interpolation and calculation of all input variables required by the dynamic driver. A configuration file with paths to the WRF output, terrain smoothing and information about the static driver used by PALM to describe the surface are set up by the user and the code outputs a ready to go dynamic driver file.

4.11 Sensitivity to boundary conditions (PALM)

The calculated input data fed to PALM from WRF can be supplied as LOD 1, where all grid points in the domain are initialized with one profile for all the input variables, or as LOD 2, where each grid point gets its own profiles [Maronga et. al. 2020]. Additionally the left, right, north, south and top faces of the domain edges are also updated in similar manner with either a single profile at each face, or different profiles at each grid point along the edges. For smaller domain configurations or more homogenous terrain LOD 1 is enough and the flow in PALM is able to adjust typically within one hour of simulated time. However, in the PALM simulations conducted for this WP we model an area around central Paris of 32 km x 32 km horizontally, and the mountainous areas surrounding central Paris can cause unwanted behaviour with LOD 1, as shown in Figure 23.

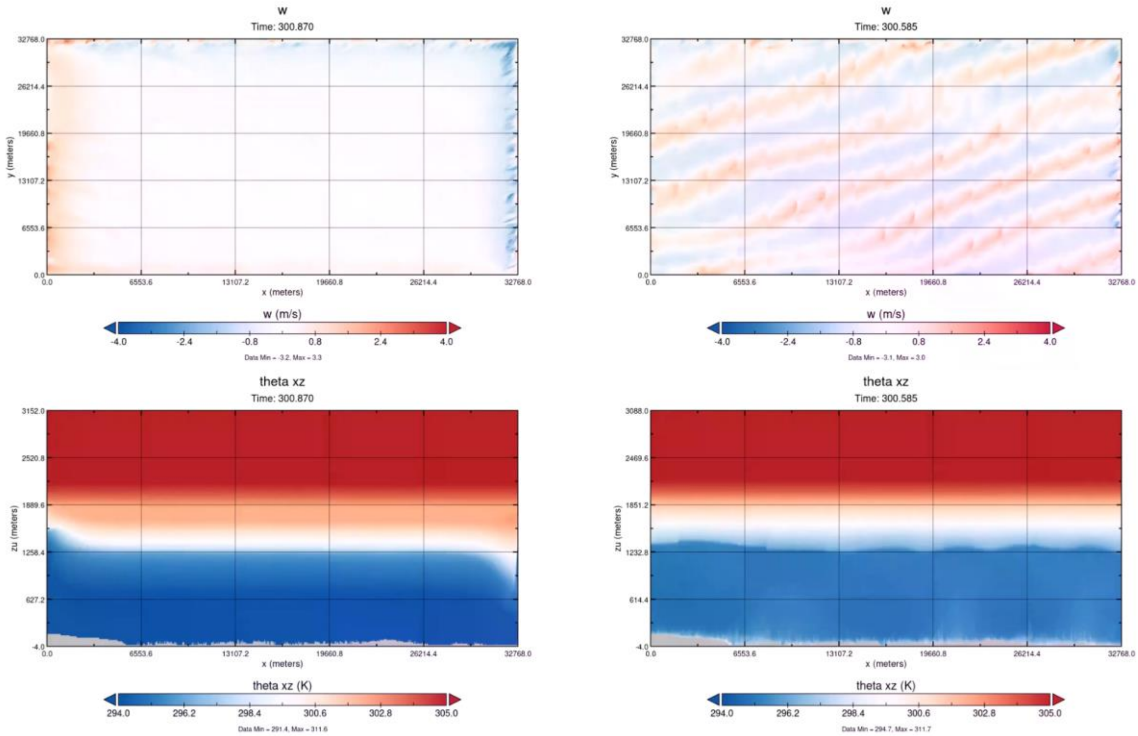

Figure 23. 5 minutes averaged PALM output in LOD 1 and 2 after 5 minutes of simulated time. Left column is PALM initialized and driven with LOD 1 boundary conditions and the right column is with LOD 2. Upper row shows the horizontal distribution of vertical wind speeds at a height of 256 meters above sea level. The lower row shows a side view of the PALM domain, or cross-section in the xz plane of potential temperature.

On the upper row we can see how the initial vertical motions are suppressed with LOD 1 initialization compared to LOD 2, where there are already convective rolls present. Additionally, there is some ascent at the left face of the domain and descent at the right face with LOD 1, whereas in LOD 2 the edge effects are less pronounced. From the bottom row we can see the terrain height as grey areas at the bottom of the figures, which leads to a vertical offset of the profiles at the left and right domain edges. This happens because the whole domain gets one profile, which takes into account the mean height of the terrain, but the left edge is higher and right edge is lower. The resulting potential temperature profiles are mismatched at both edges and it causes an internal wave to appear at time of initialization.

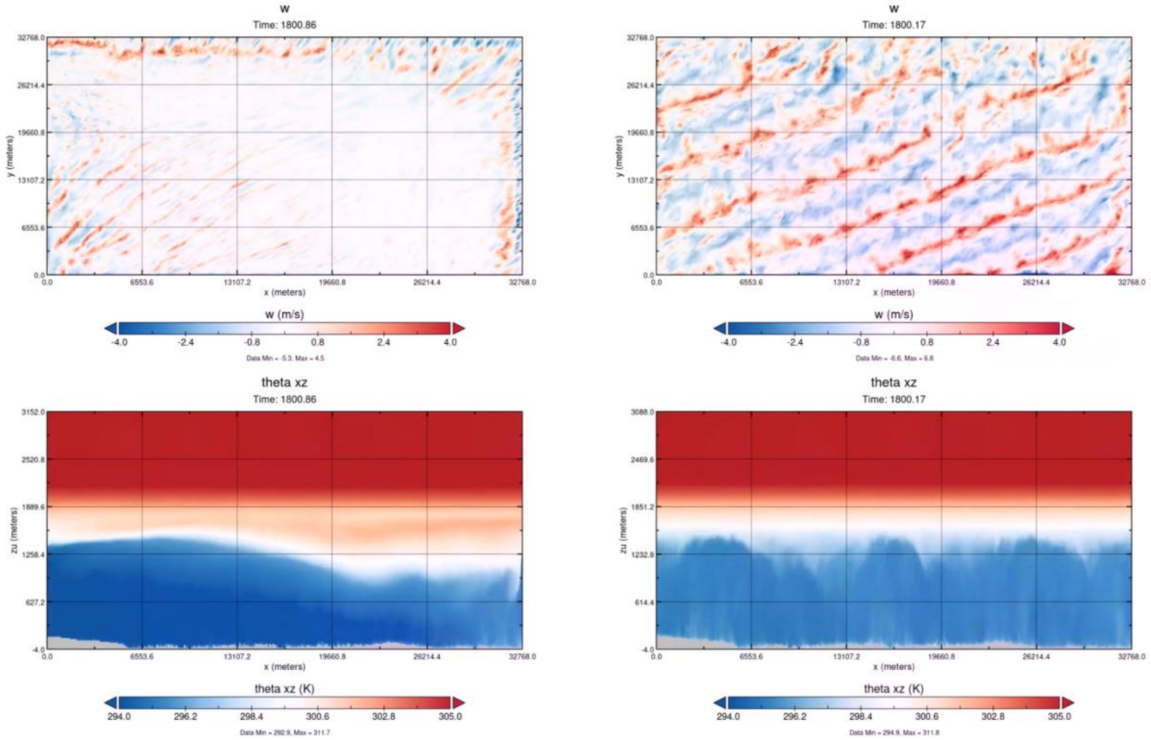

Figure 24. Same as Figure 23 but a 5 minutes averaged snapshot after 30 minutes of simulated time.

Figure 24 shows the state of the PALM simulations after 30 minutes, where the waves generated at both domain edges due to an offset of profiles have reached the midpoint of the domain, whereas LOD 2 starts to look more mature in comparison.

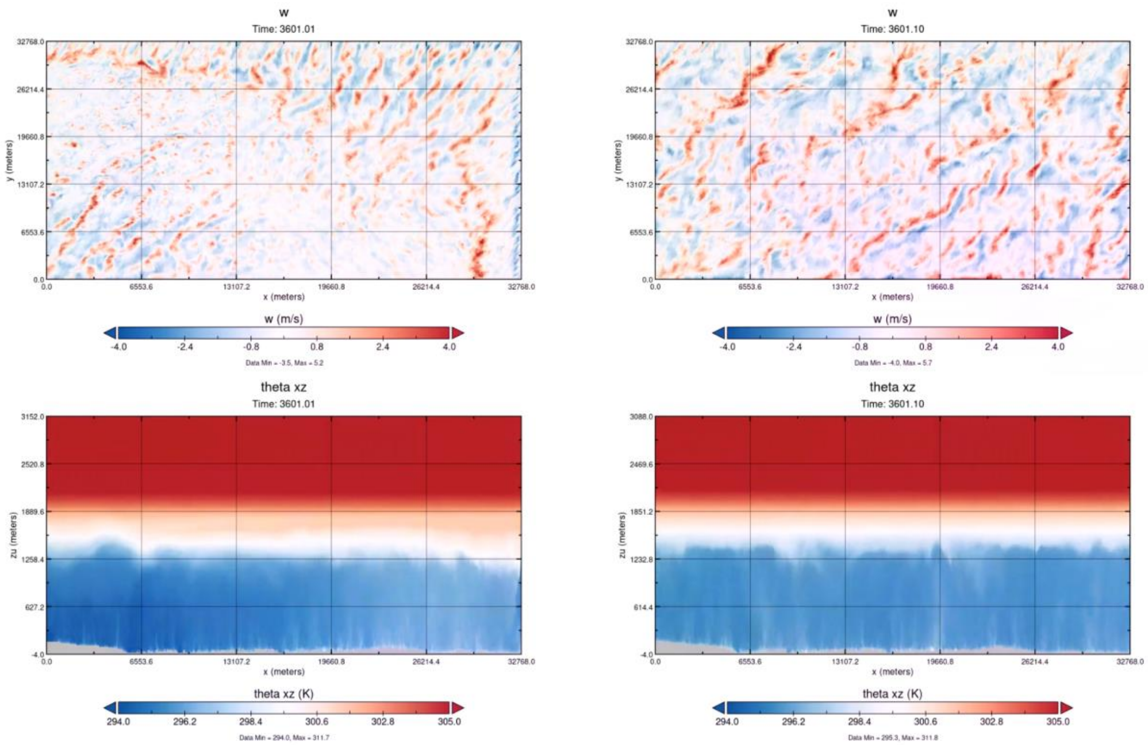

Figure 25. Same as Figure 23 but a 5 minutes averaged snapshot after 60 minutes of simulated time.

Figure 25 shows the model state after one hour of simulation. The potential temperature cross-section starts to look similar in both cases, but from the vertical motions in the upper row we can see that the model still has not adjusted to the boundary conditions with LOD 1. The linear convective rolls with LOD 2 have been disturbed and the flow has become more uniformly turbulent compared to LOD 1. The vertical wind speeds with LOD 1 show a stagnation zone in the centre of the domain, whereas LOD 2 has updrafts and downdrafts throughout the domain.

5 Conclusion

We have conducted a series of large-eddy simulations with the goal to test the sensitivity to boundary conditions in the MicroHH model. We focused on wind profiles used for nudging and wind drag caused by buildings in the domain. This work was motivated by clear differences in wind speed and direction between simulated and measured wind (Fig. 1).

For the experiments we have conducted, the simulations have proven to be quite robust in their consistency. Apart from the increased drag that caused too low winds particularly outside the city, simulations have not shown significant improvements in the simulated wind.

The reason for this is likely that we still nudge the wind towards values of one horizontally average profile. This means we are forcing a wind profile measured at one point location on the wind profile at a location 70 km away. To circumvent this problem, we could skip the nudging altogether. As an alternative, open boundary conditions (used in WRF-LES for example) could be used to force the winds in the simulations. In this case, the LES domain of high resolution is nested in a series of coarser domains. This implies that simulations can freely adjust winds to high-resolution features, such a building drag and differential heating. In other words, the influence of the boundaries (e.g. ERA5) gradually diminish moving into the high-resolution domain. Currently, a similar open boundary set-up is being tested in MicroHH.

Regarding the WRF-LES simulations, the boundary conditions are defined for all boundaries using 3D fields from re-analyses products (here GFS and ERA5). The evaluation differs from single profiles as the spatial complexity of the driver data can impact the displacement of large plumes from distant sources, and the local dynamics. Overall, despite small differences in terms of meteorology, we noticed large systematic differences in terms of CO2 concentrations (up to 20% in mean errors) which could impact the inversion of sources and sinks over the area. The use of data assimilation (4D nudging) reduces the impact of boundary conditions, as shown by the model-data differences using wind lidar profilers. We conclude here from this evaluation that the meteorological boundary conditions require data assimilation within our simulation to limit the sensitivity of external forcings. In the upcoming months, we will further evaluate the use of the IFS boundary conditions to produce high-resolution simulations consistent with large-scale forcings.

Concerning the influence of buildings on wind, drag can significantly influence wind at the location of interest. The problem identified in this work is that, while the drag force is prescribed for each grid box, a drag coefficient is uniform throughout the domain. The drag force considers how much of the grid box is occupied by a solid object. When a drag coefficient is “tuned” for a dense city, the change needed is the city centre might not be applicable to locations closer to the see. Moreover, the configurations of buildings, i.e. their density and height, may vary greatly. A solution might be to test different drag models such as a porosity-based models. Another solution would be to completely circumvent the need for the drag force parametrizations and use immersed boundaries in LES, a feature already implemented in the PALM model.

PALM requires information about the atmospheric state at initialization and regular updates at the domain boundaries. While PALM provides tools to prepare this data, careful setup is required. Boundary conditions based on LOD 1 and LOD 2 lead to different model behaviours. With LOD 1, the simulation requires a longer simulation period for the flow to adjust, consuming more time and computational resources. In contrast, LOD 2 produces more realistic wind and temperature fields earlier in the simulation and reduces initialization artifacts, such as internal waves. Overall, LOD 2 offers a more efficient and physically consistent setup, especially in complex or heterogeneous terrain.

6 References

van Heerwaarden, C. C., Van Stratum, B. J., Heus, T., Gibbs, J. A., Fedorovich, E., & Mellado, J. P. (2017). MicroHH 1.0: A computational fluid dynamics code for direct numerical simulation and large-eddy simulation of atmospheric boundary layer flows. *Geoscientific Model Development*, *10*(8), 3145-3165.

Hersbach, H., Bell, B., Berrisford, P., Hirahara, S., Horányi, A., Muñoz-Sabater, J., ... & Thépaut, J. N. (2020). The ERA5 global reanalysis. *Quarterly Journal of the Royal Meteorological Society*, *146*(730), 1999-2049.

Inness, A., Ades, M., Agustí-Panareda, A., Barré, J., Benedictow, A., Blechschmidt, A. M., ... & Suttie, M. (2019). The CAMS reanalysis of atmospheric composition. *Atmospheric Chemistry and Physics*, *19*(6), 3515-3556.

Krol, M., van Stratum, B., Anglou, I., & Boersma, K. F. (2024). Evaluating NO x stack plume emissions using a high-resolution atmospheric chemistry model and satellite-derived NO 2 columns. *Atmospheric Chemistry and Physics*, *24*(14), 8243-8262.

Lilly, D. K. (1996). A comparison of incompressible, anelastic and Boussinesq dynamics. *Atmospheric research*, *40*(2-4), 143-151.

Ražnjević, A., van Heerwaarden, C., and Krol, M. (2022)a. Evaluation of two common source estimation measurement strategies using large-eddy simulation of plume dispersion under neutral atmospheric conditions, Atmos. Meas. Tech., 15, 3611–3628, https://doi.org/10.5194/amt-15-3611-2022, 2022.

Ražnjević, A., Van Heerwaarden, C., Van Stratum, B., Hensen, A., Velzeboer, I., Van Den Bulk, P., & Krol, M. (2022)b. Interpretation of field observations of point-source methane plume using observation-driven large-eddy simulations. *Atmospheric Chemistry and Physics*, *22*(10), 6489-6505.

van Stratum, B. J. H., van Heerwaarden, C. C., & Vilà-Guerau de Arellano, J. (2023). The Benefits and Challenges of Downscaling a Global Reanalysis With Doubly-Periodic Large-Eddy Simulations. *Journal of Advances in Modeling Earth Systems*, *15*(10), e2023MS003750.

Stull, R. B. (2012). *An introduction to boundary layer meteorology* (Vol. 13). Springer Science & Business Media.

Zhang, M., Carlo, O., Peng, Y., Gao, Z., Zhang, J., Ji, G., & Buccolieri, R. (2025). Volumetric drag coefficients for generic urban configurations: Insights from canopy flow analysis. *Building and Environment*, *267*, 112273.

Document History

Version	Author(s)	Date	Changes
0.1 (Initial document created)	Thomas Lavaux, Leena Jarvi, Jani Stromberg	April 2025	
0.2	Thomas Lavaux, Leena Jarvi, Jani Stromberg		Version for internal project review
1.0	As above	20 May 2025	Issued version

Internal Review History

Internal Reviewers	Date	Comments
Sylvie Malardel (MF), Frederic Chevallier (CEA)	April 2025	